Focusing of fast transverse modes in (001) silicon at ultrasonic frequencies

Kwang Yul Kim, Arthur G. Every and Wolfgang Sachse

Citation: The Journal of the Acoustical Society of America **95**, 1942 (1994); doi: 10.1121/1.408708
View online: https://doi.org/10.1121/1.408708
View Table of Contents: https://asa.scitation.org/toc/jas/95/4
Published by the Acoustical Society of America

Focusing of fast transverse modes in (001) silicon at ultrasonic frequencies

Kwang Yul Kim
Department of Theoretical and Applied Mechanics, Thurston Hall, Cornell University, Ithaca, New York 14853

Arthur G. Every
Department of Physics, University of the Witwatersrand, Johannesburg, South Africa

Wolfgang Sachse
Department of Theoretical and Applied Mechanics, Thurston Hall, Cornell University, Ithaca, New York 14853

(Received 12 October 1993; accepted for publication 13 December 1993)

This paper presents observations of the focusing of fast transverse (FT) ultrasonic waves in a (001) oriented, disk-shaped silicon single crystal. These modes are almost perfectly shear horizontally (SH) polarized and were absent from earlier reported observations of focusing of ultrasonic waves based on axisymmetric excitation and sensing. In an experiment the FT modes are generated and detected at room temperature by two small [100] polarized PZT piezoelectric shear transducers. The source transducer is fixed on the bottom surface of the specimen and the detector scans the top surface in the [100] direction along lines that intersect the [010] axis at various distances from epicenter. The observed focusing pattern indicates a strong concentration of the FT mode flux in a narrow band about the (100) plane containing the source. Because of the specific way in which the monopolar source acts, the radiated acoustic flux pattern breaks the fourfold symmetry associated with cubic media. While it shows a strong concentration of FT flux toward the (100) plane, it suppresses FT modes propagating very near the (010) plane passing through the source. The spatial variation of the Fourier components of the detected signal at approximately 2, 6, and 8 MHz has been examined, and there is good accountability for this variation on the basis of the computed frequency domain elastodynamic Green's function for silicon.

PACS numbers: 43.35.Cg, 43.35.Ty

INTRODUCTION

There has been significant progress recently in developing an understanding of the dynamic response of elastically anisotropic solids at ultrasonic frequencies. Thermal phonon imaging paved the way for this by revealing the intricate nature of phonon focusing in crystals.[1–5] The phenomena observed at thermal phonon and at ultrasonic frequencies differ in some important respects, however. Central to this paper is the issue of polarization selectivity, which we discuss in the context of its effect on the focusing pattern of silicon. Whereas thermal phonon sources and detectors tend to be polarization insensitive, ultrasonic transducers are by and large polarization selective in their mode of excitation and detection. In ballistic phonon imaging it is a scalar quantity, the temperature or thermal energy density, that is propagated as a heat pulse,[6] whereas in ultrasonic experiments it is the vector displacement field that is coupled to, and thereby the dynamic Green's function tensor or its spatial derivatives that are probed. The mode of transduction, whether, for example, it is axisymmetric or polarized parallel to the sample surface, is critical in determining which components of this tensor are measured. A second important distinction between thermal phonon and ultrasonic imaging arises from the fact that ultrasonic wavelengths are orders of magnitude greater than those of thermal phonons. Because of the short wavelengths of thermal phonons, their phonon focusing patterns and the caustics they contain are well accounted for on the basis of the ray approximation of geometrical acoustics.[1–5] In a number of ultrasonic experiments that have been performed recently,[7–14] on the other hand, although the distance from source to detector is still significantly greater than the dominant wavelength of the transmitted acoustic signals, the asymptotic far-field condition is not as well satisfied, and the caustics are diffraction broadened. In the process much of the fine structure of the caustic patterns is lost and, in the case of narrow-band signals, replaced by a pattern of diffraction fringes.[9–11] The interpretation of these diffraction patterns involves a consideration of the precise elastodynamic Green's functions for the medium, which goes well beyond the ray approximation.[15–26]

As a lead in and motivation for our investigations we recall some recent findings. Three years ago we reported the focusing and mode conversion of slow transverse (ST) mode elastic waves generated thermoelastically by laser irradiation in a disc shaped (100) oriented silicon crystal.[7,8] The elastic waves were detected with a small longitudinal (L) PZT transducer attached to the surface opposite to the source. Focusing and internal diffraction of

 0001-4966/94/95(4)/1942/11/$6.00

ST waves in several (100) oriented cubic single crystals have been reported by Hauser *et al.*,[9,10] who used two water immersion focusing L transducers for insonification and detection. Similar experiments have been carried out by Wesner *et al.*[11] on a number of other crystals. Phonon focusing of surface acoustic waves (SAW) generated by pulsed laser excitation of a silicon wafer has been reported by Kolomenskii and Maznev.[12] Recently, Kim *et al.*[13,14] have reported the focusing of ST modes in a (0001) oriented zinc specimen, observed with various combinations of source and detector, such as capillary fracture and capacitive displacement detector, miniature piezoelectric PZT source and detector, and laser scan source and piezoelectric PZT detector.

A common feature of the sources of ultrasound and systems being studied in the experiments mentioned above is that they correspond to axisymmetric excitation of media in which the modes to a good approximation can be classified as either sagittally or shear horizontally (SH) polarized. In most cases the detection sensitivity is also axisymmetric. In this situation only the sagittally polarized modes can be observed. On grounds of symmetry the SH modes can neither be excited nor detected. In the case of (001)-oriented silicon, it is the fast transverse (FT) modes that are very nearly SH polarized, while for (0001) oriented zinc the FT modes are pure SH. For this reason only the slow transverse (ST) and longitudinal (L) modes and related surface and head waves have been observed in the above mentioned experiments, and there is no visible presence of FT modes.

In the experiment we report here, in place of axisymmetric excitation and sensing we have used small piezoelectric shear transducers as source and sensor. These have allowed us to observe the intense focusing of SH polarized FT acoustic waves near the (100) plane in a (001) oriented silicon single crystal. By examining different Fourier components of the transmitted signal we are able to show clearly how the diffraction broadened focusing pattern varies with frequency. Our observations are in good agreement with the computed Green's function for the medium.

I. THEORY

A. Polarization field, slowness surface, and focusing of FT modes in silicon

Widespread use is made of representational surfaces and other graphical devices to describe the directional dependence of the acoustic slowness, phase and group velocities and mode polarization vectors in anisotropic solids.[27,28] Our discussion will be mainly restricted to fast transverse modes in silicon. Figure 1 depicts the polarization patterns for the FT and ST modes of silicon near the [001] direction. In the {100} symmetry planes, and also in the {110} symmetry planes out as far as the ⟨111⟩ directions which make an angle of 54.7° with the [001] axis, the FT modes are pure transverse and therefore SH polarized. In the region between these two sets of planes the polarization pattern for the FT modes remains very nearly SH.

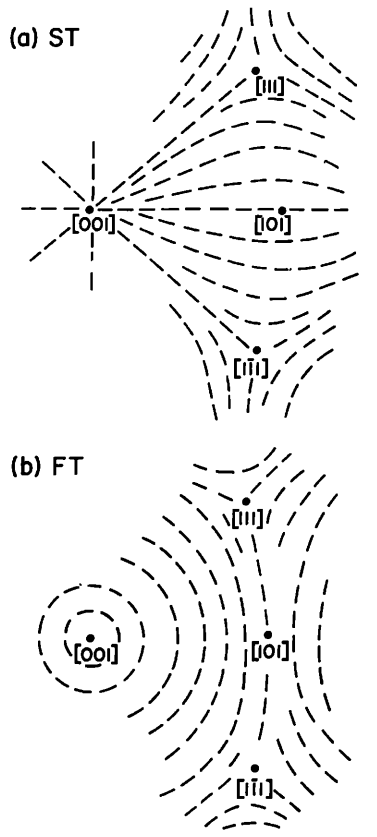

FIG. 1. Polarization patterns for the FT and ST modes in silicon.

The L and ST modes, on the other hand, are throughout either exactly or very nearly sagittally polarized.

The group or ray velocity $\mathbf{V}_g$ is obtained from the relation[27]

$$\mathbf{V}_g \equiv \nabla_{\mathbf{k}}\omega = \nabla_{\mathbf{n}} v = \frac{\nabla_{\mathbf{s}} S}{\mathbf{s}\cdot\nabla_{\mathbf{s}} S}, \tag{1}$$

where ω is the angular frequency, $\mathbf{k}$ is the wave vector, $\mathbf{n}=\mathbf{k}/|\mathbf{k}|$ is the wave normal, v is the phase velocity, $\mathbf{s}$ is the slowness defined as $\mathbf{n}/v$, and S is the equation of the slowness surface. The above equation indicates that the outward normal to the slowness surface at any point is the direction of the group or energy velocity of the corresponding mode. Figure 2 shows the FT sheet of the slowness surface in silicon. Near each {100} plane this surface has a very shallow saddle shape, being convex and circular in the plane with a radius $(\rho/C_{44})^{1/2}$ and concave across the plane. On either side of the {100} type plane, not far off, there are lines of zero curvature, denoted by bold line, that converge on the ⟨100⟩ directions. Beyond these lines both principal curvatures of the surface are convex. Beyond each of these lines of zero curvatures, there is a line, also converging on the ⟨100⟩ directions, on which the surface normals lie in the {100} plane. Due to this particular shape of the slowness surface, the FT sheet of the group velocity surface is folded across the {100} plane, and its section in this plane, which is shown in Fig. 3, consists of two curves: one is a circle of radius $(C_{44}/\rho)^{1/2}$ and the other is a curve

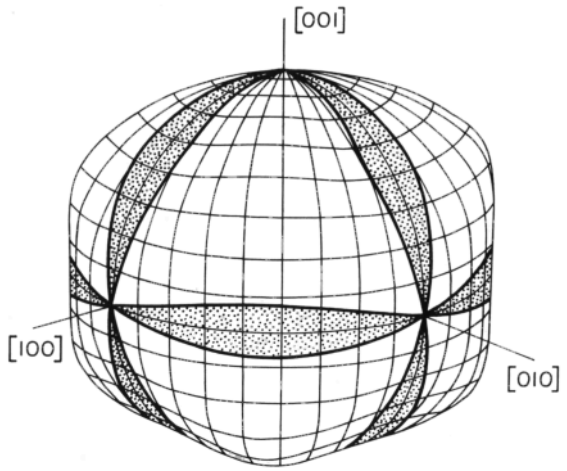

FIG. 2. FT sheet of the slowness surface in silicon. The bold lines bordering the shaded saddle shaped regions are where the Gaussian curvature is zero.

that lies indistinguishably close to this circle within the time resolution of our experiment.

Because of the nonspherical shape of the slowness surface in anisotropic media including silicon, the ray vectors are more strongly clustered (focused) in some directions than in others and this results in pronounced nonuniformity in the energy flux. A parameter that provides a good measure of focusing is the Maris phonon enhancement factor A defined as[1]

$$A \equiv \delta\Omega_s/\delta\Omega_v, \tag{2}$$

where $\delta\Omega_s$ is the infinitesimal solid angle subtended by a small cluster of slowness vectors and $\delta\Omega_v$ is the solid angle subtended by their associated ray vectors. A can be shown to be related to the Gaussian curvature $K=L_1L_2$, where L_1 and L_2 are the two principal curvatures of the slowness surface, by

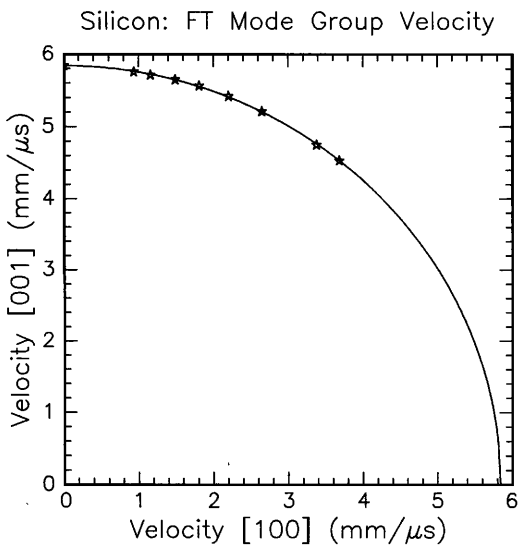

FIG. 3. (100) section of the FT sheet of the group velocity surface, with stars denoting experimental data.

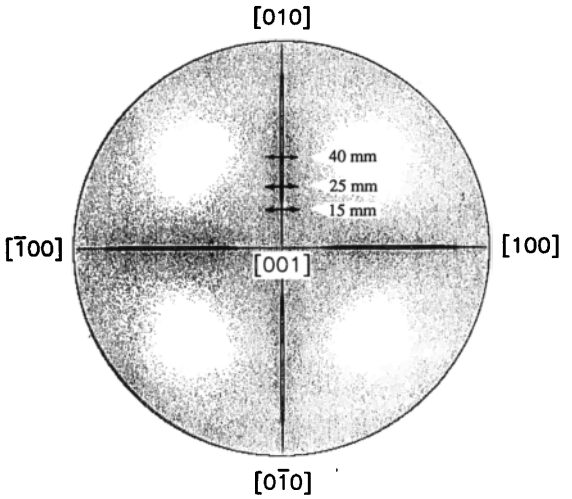

FIG. 4. Theoretical polar plot of the FT focusing pattern in silicon corresponding to a uniform distribution of wave normals. Three scan lines are indicated by the bidirectional arrows.

$$A = 1/(s^3 V_g |K|). \tag{3}$$

It follows from Eq. (3) that the lines of zero curvature on the slowness surface map onto caustics, where the energy flux is infinite. Figure 4 is a Monte Carlo generated polar plot of the energy focusing pattern for silicon, based on the assumption of a uniform distribution of wave normals **n** in all directions. The theory predicts strong FT focusing in narrow bands about the {100} planes, bounded by a pair of caustics which straddle each such plane and converge on the ⟨100⟩ directions. These caustics are associated with the lines of zero curvature in Fig. 2. This focusing pattern is in excellent agreement with the observed focusing of ballistic phonons at 2° K[29] and in essential agreement with our observation to be described in the next section. In each ⟨111⟩ direction there is a conical point and the FT slowness sheet has an undefined normal, the direction of which depends on the direction of approach on the slowness surface toward that ⟨111⟩. As a result, the FT sheet of the group velocity surface has lacuna or missing circular patches of half-angle 12.6° when viewed from the origin. This phenomenon is known as internal conical refraction. The cones project on the polar plot of Fig. 4 as blank white regions centered on the {110} type planes and located at roughly two-thirds of the distance from the origin to the circumference.

Although the individual caustics alongside the {100} planes are well resolved in thermal imaging,[29] in our experiment, because of the much larger characteristic wavelength at ultrasonic frequencies, the caustics are diffraction broadened to the extent that they merge into a single broad ridge. Furthermore, the excitation in our experiment takes place in the [100] direction, which results in strongest SH generation near the (100) plane and little excitation of the SH modes near the (010) plane. A striking consequence of this anisotropic distribution of wave normals is the sup-

pression of the FT mode focusing near the (010) plane. To delve further into these phenomena, we consider next the elastodynamic Green's functions of silicon and their spatial and frequency dependence.

B. Elastodynamic Green's functions

In our experiment the silicon sample is oriented in the (001) symmetry plane. Within the scan range of the detector, all the FT modes are SH and parallel to the sample surface. The (001) sample surface plays only a minor role, since negligible mode conversion takes place there between the FT modes and the L and ST modes. For this reason too, there is no compulsive need to consider head wave effects. An adequate explanation of the observations is arrived at by considering the infinite elastic continuum Green's function for silicon. Let $\tilde{G}_{sp}(\mathbf{x},t)$ represent the s'th component of the displacement at point $\mathbf{x}$ and time t in response to a point force in the p'th direction with time dependence $F(t)$, applied at the origin. $\tilde{G}_{sp}(\mathbf{x},t)$ and $F(t)$ are related by the Cauchy–Navier equation for an anisotropic medium:

$$\left(\rho\delta_{rp}\frac{\partial^2}{\partial t^2}-C_{rlsm}\frac{\partial^2}{\partial x_l\partial x_m}\right)\tilde{G}_{sp}(\mathbf{x},t)=\delta_{rp}\delta(\mathbf{x})F(t). \quad (4)$$

In the special case of $F(t)$ being the impulse function $\delta(t)$, $\tilde{G}_{sp}(\mathbf{x},t)$ become Green's functions. The array of Green's functions forms a tensor of second rank.

The formal solution to Eq. (4) in terms of integral transforms has been considered by a number of authors,[15–21] and there have been several books and reviews on the subject.[22–25] Carrying out a quadruple space-time Fourier transform on Eq. (4), one obtains

$$L_{rs}(\mathbf{k},\omega)\tilde{g}_{sp}(\mathbf{k},\omega)=\frac{1}{(2\pi)^3}\delta_{rp}f(\omega), \quad (5)$$

where

$$f(\omega)=\frac{1}{2\pi}\int F(t)e^{i\omega t}\,dt, \quad (6)$$

$$L_{rs}(\mathbf{k},\omega)=C_{rlsm}k_lk_m-\rho\omega^2\delta_{rs}, \quad (7)$$

and

$$\tilde{g}_{sp}(\mathbf{k},\omega)=\frac{1}{(2\pi)^4}\int d^3\mathbf{x}\,dt\tilde{G}_{sp}(\mathbf{x},t)e^{-i(\mathbf{k}\cdot\mathbf{x}-\omega t)}. \quad (8)$$

From Eq. (5) it follows that

$$\tilde{g}_{sp}(\mathbf{k},\omega)=\frac{1}{(2\pi)^3}[L^{-1}(\mathbf{k},\omega)]_{sp}f(\omega)=g_{sp}(\mathbf{k},\omega)f(\omega), \quad (9)$$

which defines the Fourier domain Green's function $g_{sp}(\mathbf{k},\omega)$, whose inverse Fourier transform with respect to $\mathbf{k}$ is

$$G_{sp}(\mathbf{x},\omega)=\frac{1}{(2\pi)^3}\int d^3\mathbf{k}[L^{-1}(\mathbf{k},\omega)]_{sp}e^{i\mathbf{k}\cdot\mathbf{x}}. \quad (10)$$

Combining Eqs. (9) with (10) and inverse Fourier transforming with respect to t, we obtain

$$\tilde{G}_{sp}(\mathbf{x},t)=\int G_{sp}(\mathbf{x},\omega)f(\omega)e^{-i\omega t}\,d\omega. \quad (11)$$

Using the spectral resolution theorem,[19] we can write

$$(L^{-1})_{sp}=\sum_n\frac{\Lambda_{sp}^{(n)}}{\rho v^{(n)2}k^2-\rho\omega^2}=\sum_n\frac{s^{(n)2}\Lambda_{sp}^{(n)}}{\rho(k^2-\omega^2s^{(n)2})}, \quad (12)$$

where the sum is taken over the three eigenvalues $\rho v^{(n)2}k^2$ of the tensor $\Gamma_{rs}=C_{rlsm}k_lk_m$, $v^{(n)}$ is the phase velocity, and $s^{(n)}=1/v^{(n)}$ the slowness, $\Lambda_{sp}^{(n)}=U_s^{(n)}U_p^{(n)}$, and $\mathbf{U}^{(n)}$ is the eigenvector associated with $\rho v^{(n)2}k^2$. In performing the integration in Eq. (10), it is convenient to orient the k_3 axis in the direction of $\mathbf{x}$ and transform to polar coordinates so that $\mathbf{k}=k(\sin\theta\cos\varphi,\sin\theta\sin\varphi,\cos\theta)$ and $d^3\mathbf{k}\rightarrow d\Omega k^2\,dk$, where $d\Omega=d(\cos\theta)d\varphi$ is the element of solid angle in k space. Integration with respect to k is facilitated by taking the limits to be $-\infty$ to ∞ rather than 0 to ∞, and to compensate, the angular integral is taken only over the forward hemisphere such that $\cos\theta\geqslant 0$, rather than over the entire sphere. Thus one obtains

$$G_{sp}(\mathbf{x},\omega)=\frac{1}{8\pi^3\rho}\sum_n\int_\Omega d\Omega s^{(n)2}\Lambda_{sp}^{(n)}\times\int_{-\infty}^{\infty}\frac{e^{ikx\cos\theta}k^2\,dk}{(k^2-\omega^2s^{(n)2})}, \quad (13)$$

where $x=|\mathbf{x}|$. The poles that are encountered in the k integral are handled by ascribing a small imaginary part $i\epsilon$ to ω, corresponding to the slow switching on of the force. The path of integration is then completed in the upper or lower half complex plane depending on the sign of $x\cos\theta$. This leads through the identity

$$\int_{-\infty}^{\infty}\frac{e^{iku}k^2\,dk}{(k^2-a^2)}=\pi iae^{ia|u|}+2\pi\delta(u), \quad (14)$$

to the following result:

$$G_{sp}(\mathbf{x},\omega)=\sum_n\left[\frac{i\omega}{8\pi^2\rho}\int_\Omega d\Omega s^{(n)3}\Lambda_{sp}^{(n)}e^{i\omega s^{(n)}x\cos\theta}+\frac{1}{8\pi^2\rho x}\int_0^{2\pi}d\varphi s^{(n)2}\Lambda_{sp}^{(n)}\right]. \quad (15)$$

The second integral is taken over the circle for which $\cos\theta=0$. For isotropic solids the angular integrals can be performed analytically, leading to Eq. (4.35) of Aki and Richards.[26] In the case of anisotropic solids, except for certain special cases where analytic results are known, the angular integrals have to be performed numerically. The first term in Eq. (15), because it involves 2-D integration, is the most CPU intensive, and it is the rapid variation in the phase factor that tends to be the crucial consideration. One chooses a rectangular grid of points in the variables φ and $\cos\theta$ to sum over, with the spacing small enough that the variation of $\omega sx\cos\theta$ between neighboring grid points is much smaller than 2π. At relatively low frequencies such that $\omega sx<10\pi$ say, the numerical summation requires a modest amount of CPU time. At higher frequencies, where the grid size needs to be small, the numerical integration is

made manageable by invoking the stationary phase approximation, and limiting the summation to small regions around directions where the phase $\omega sx\cos\theta=\omega\mathbf{s}\cdot\mathbf{x}$ is stationary. These correspond to points on the slowness surface where the outgoing normal and hence group velocity $\mathbf{V}$ are parallel to $\mathbf{x}$. At very high frequencies these regions shrink to a very small size, within which the factor $s^3\Lambda$ can be taken to be a constant, and the equation for the slowness surface approximated by $s_3=L_1s_1^2+L_2s_2^2$ in a locally oriented coordinate system, where L_1 and L_2 are the local principal curvatures. The integral can now be performed analytically yielding a contribution to $G_{sp}(\mathbf{x},\omega)$ of the form

$$G\approx\frac{\Lambda e^{i\omega\mathbf{s}\cdot\mathbf{x}}}{\sqrt{|L_1L_2|}}, \tag{16}$$

for each such point. The intensity or energy flux associated with each contribution is proportional to $|G|^2$, and is thus inversely proportional to $|K|=|L_1L_2|$, the magnitude of the Gaussian curvature of the slowness surface. This is precisely what is predicted on the basis of the ray approximation, as shown in Eq. (3).

In our experiment the piezoelectric shear source located at the origin acts in the [100] direction and the shear detector, which senses displacements in the [100] direction, is scanned in position. The source acting on the sample surface with the time function $F(t)$ appearing in Eq. (4) is modeled as a monopolar force directed in the [100] direction and it is delivered to the specimen through a coupling medium from the piezoelectric transducer at the origin. The output voltage $V(\mathbf{x},t)$ of the detector corresponds to the horizontal surface displacement of the sample. The transfer function $T(\mathbf{x},t)$ between the surface displacement $\tilde{G}_{11}(\mathbf{x},t)$ and $V(\mathbf{x},t)$ is a scalar function, which is assumed to be independent of the position $\mathbf{x}$. This is true when the coupling film between the sample and the detector is uniform over the various positions under the uniform pressure applied to the detector. This assumption turns out to hold very well in our experiment described in the next section. $V(\mathbf{x},t)$ is then related to $\tilde{G}_{11}(\mathbf{x},t)$ through a convolution integral

$$V(\mathbf{x},t)=\tilde{G}_{11}(\mathbf{x},t)*T(t), \tag{17}$$

where $*$ denotes the operation of the convolution integral. Taking the temporal Fourier transform of Eq. (17) with the help of Eq. (11) yields

$$\mathcal{V}(\mathbf{x},\omega)=f(\omega)\tau(\omega)G_{11}(\mathbf{x},\omega), \tag{18}$$

where $\mathcal{V}(\mathbf{x},\omega)$ and $\tau(\omega)$ are the Fourier transforms of $V(\mathbf{x},t)$ and $T(t)$, respectively. Equation (18) indicates that the spatial variation of the Fourier spectrum of the detector output at a particular frequency follows that of the Green's function, $G_{11}(\mathbf{x},\omega)$, at that frequency.

Figure 5 shows the computed spatial variation of the Green's function component $G_{11}(\mathbf{x},\omega)$ in the $x_3=49.15$-mm plane for frequency $f=2$ MHz, with darkness representing the magnitude of G; 49.15 mm is the thickness of the sample. Only the contribution of the FT modes has been included in the calculation. Starting at very high frequency, as the frequency is lowered, the FT

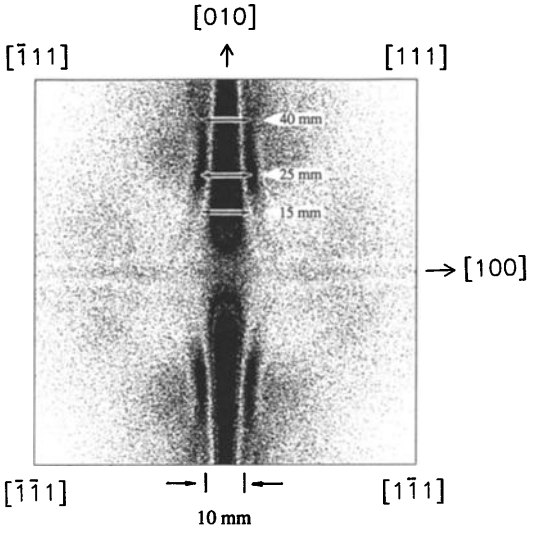

FIG. 5. Computed spatial variation of $G_{11}(\mathbf{x},\omega)$ at 2 MHz on the $x_2=15$, 25, and 40 mm on the $x_3=49.15$-mm plane.

line caustics unfold into Airy diffraction patterns. The fringes broaden and eventually merge, becoming fewer in number as the frequency is lowered further. By 2 MHz only the central intense fringe and a single pair of side fringes is clearly in evidence.

Due to the fact that (100) is a preferred axis in the (001) plane, the fourfold symmetry about the [001] axis has been broken. Through the factor $\Lambda_{11}^{FT}=(U_1^{FT})^2\approx\cos^2\varphi$, the FT modes that contribute most strongly to $G_{11}(\mathbf{x},\omega)$ are those with wave normals lying close to the (100) plane, whereas those with wave normals near the (010) plane contribute negligibly. As a result the FT focusing structure near the (100) plane is very prominent, while that near the (0$\bar{1}$0) plane is almost totally suppressed. Since, moreover, $\tilde{G}_{12}=0$ on the (010) plane on grounds of symmetry, and the SH polarized FT modes do not contribute to $\tilde{G}_{13}$, it follows that the FT modes are virtually unobservable by any means very near or on the (010) plane passing through the origin. Accordingly, the scanning of the detector in our experiment is made only across the (100) plane passing through the origin.

II. EXPERIMENTAL METHOD

Figure 6 shows a schematic of our experimental set up, in which two piezoelectric PZT shear transducers are used to study the transmission of SH polarized ultrasonic waves through a sample, one transducer acting as a source and the other as a detector. The specimen studied was a (001) oriented, disc-shaped silicon single crystal of thickness 49.15 mm and diameter 100 mm. The source is located at the origin on the bottom side and the position of the detector on the upper surface is specified by the angles θ and φ, which denote the latitude measured from the [001] direction and the longitude measured from the [010] axis, respectively. The excitation and sensing elements of the source and detecting transducers were 0.75-mm-diam circular disks. They were nearly identical in nature and both polarized in the [100] direction. The source was fixed,

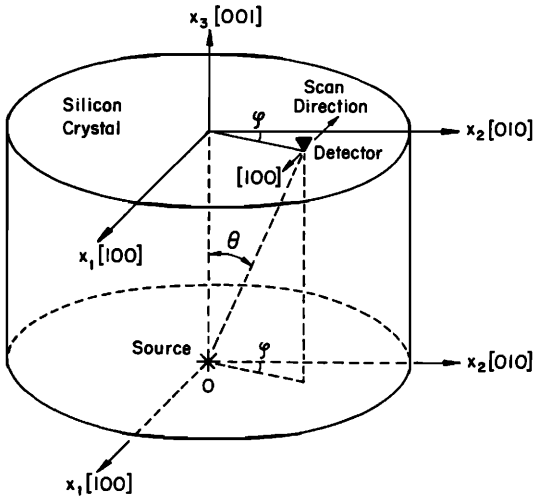

FIG. 6. Schematic of the experimental setup.

while the detector was scanned in the [100] direction along three lines which intersect the [010] axis passing through epicenter at 15, 25, and 40 mm from the epicenter. The scan range was a 6-mm interval on either side of the [010] axis. The three scan lines are drawn in Figs. 4 and 5 as the bidirectional arrows across the [010] axis.

The source was activated by a high-voltage pulse derived from the product of Panametrics, Inc., model 5055PR. The detected signal was amplified with 60-dB gain by an amplifier the bandwidth of which extended from 20 kHz to 2 MHz. The amplified output was fed into a digitizer that sampled it at a 60-MHz rate. The output of the digitizer was connected to an x-y scope for visual display of the signal and also brought into a microcomputer for storage of data and subsequent signal processing.

To compare the results of the FT mode focusing in silicon with those of SH modes observed in an isotropic medium that does not exhibit a focusing behavior, a similar experiment was performed with a 25.5-mm-thick glass plate for various detector orientations φ at constant θ.

III. RESULTS

As mentioned in the previous section and Fig. 1, this detector arrangement relative to that of the source favors the transmission of SH waves, which for directions close to the (100) plane are the FT modes. No signal corresponding to L or ST modes propagating from the source to the detector was found near the (100) plane. Further confirmation was provided by the fact that, when the detector was rotated by 90° so that its polarization direction was parallel to the [010] direction, which lies in the sagittal plane, the amplitude of the detected signal decreased to a noise level. It is also noted that when the detector was scanned across the [100] axis of the top surface, because then both source and detector were in this situation sagittally polarized, hardly any FT signal was observed. In what follows, this paper describes the strong focusing of FT waves in directions contained in a narrow band surrounding the (100) plane passing through the origin.

Shown in Fig. 3 are the measured group velocity data of the pure FT modes in various directions in the (100) plane. The arrival time of the first signal of these FT waves above the noise level was used to calculate the group velocities. These FT waves are all found to propagate with velocities nearly equal to $(C_{44}/\rho)^{1/2}$, regardless of their θ orientation. This is consistent with the (100) FT slowness section which forms a circle of radius $(\rho/C_{44})^{1/2}$ and in excellent agreement with the (100) folded theoretical FT group velocity section as described in Sec. I.

Some of the waveforms obtained when the detector was scanned across the 40-mm position on the [010] axis are displayed in Fig. 7, where the x value written on top of each waveform indicates the distance of the detector from the [010] axis passing through the epicenter of the top

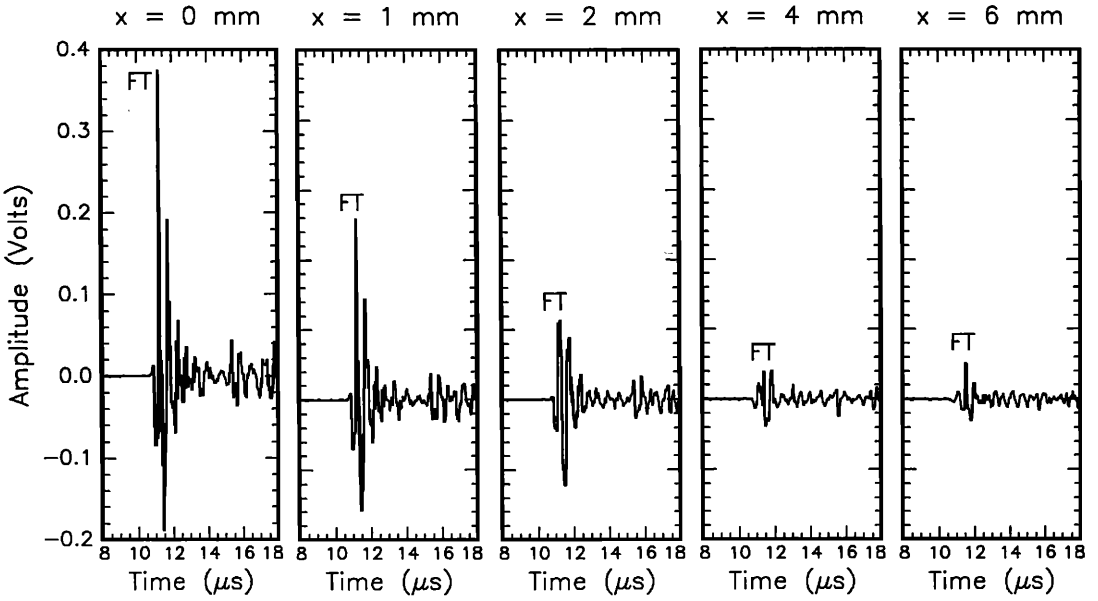

FIG. 7. Observed waveforms at various locations on the scan line at 40 mm from epicenter.

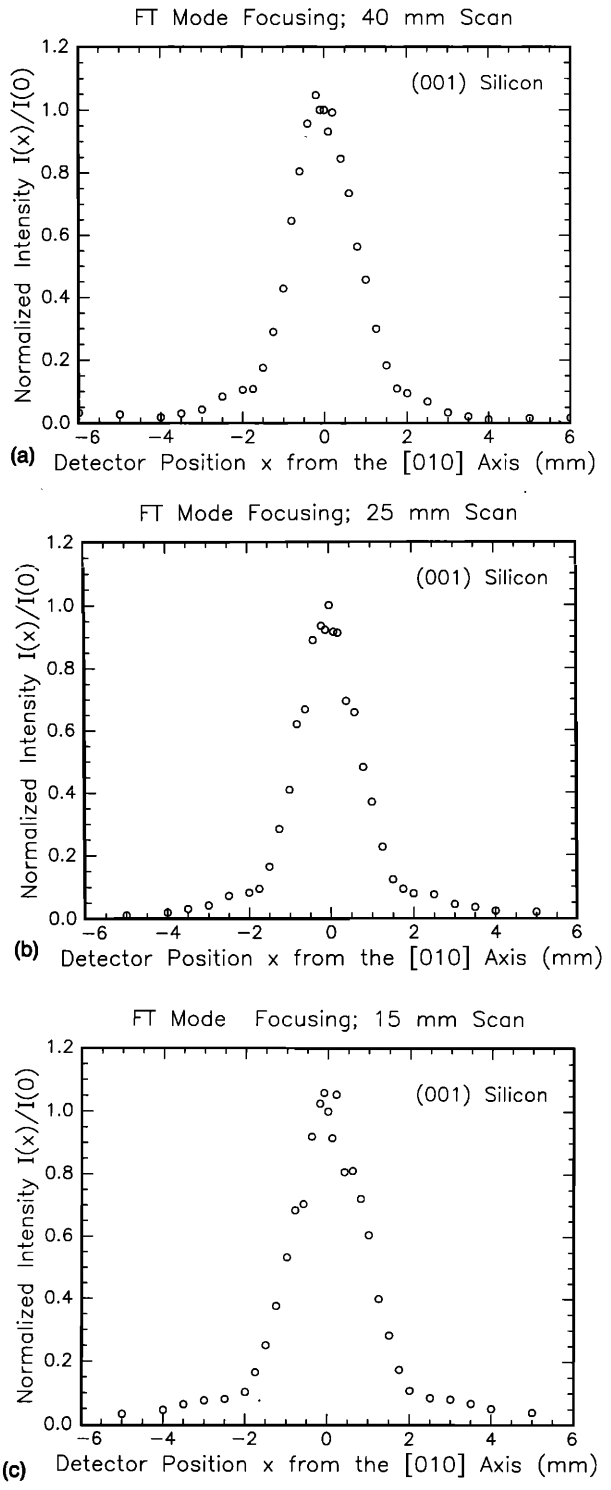

FIG. 8. Observed FT mode focusing patterns in silicon near the (100) plane: (a) detector at 40 mm, (b) detector at 25 mm, and (c) detector at 15 mm.

surface. Note the rapid change in magnitude of the observed FT amplitude as the detector moves a small distance from the [010] axis. The focusing behavior exhibited in Fig. 7 is illustrated in a graphical form in Fig. 8(a) which shows normalized intensity $I(x)/I(0)$ as a function of x. The square of the peak amplitude immediately after the arrival of the FT mode was used as a measure of intensity. The 2-mm half-width of the approximately Gaussian curve subtends an angle of 1.8°, when viewed from the source. Displayed in Fig. 8(b) and (c) are very similar focusing patterns obtained when the detector was scanned across two other positions on the [010] axis at distances of 25 and 15 mm from the epicenter. The focusing patterns observed at the three positions on the [010] axis indicate that focusing is essentially confined to the narrow band surrounding the (100) plane in good qualitative agreement with a focusing behavior shown in Fig. 4.

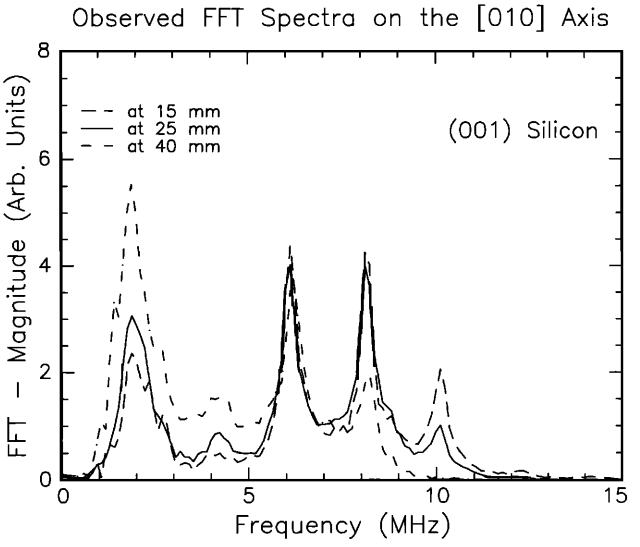

FIG. 9. Fourier magnitude spectra of three observed signals on the [010] axis.

As can be seen in Fig. 4, the theory of phonon focusing predicts that the focusing band gradually narrows down to zero in the ⟨100⟩ direction. It also predicts that the focusing is highest on the caustics on either side of each {100} plane with a dip in intensity occurring in the narrow region between the caustics. In contrast, all the experimental curves in Fig. 8(a)–(c) display a single intensity peak at the center. Moreover, a close look at their half-widths of these approximately Gaussian curves reveals that the half-width of the curve at the 15-mm detector position is slightly wider than the corresponding half-widths at 25- and 40-mm detector positions, again in contradiction with the theory of phonon focusing. This is due to the effect of diffraction broadening, which is significant at ultrasonic frequencies because of the much larger characteristic wavelength. The caustics are diffraction broadened to the extent that they merge into a single broad peak of roughly Gaussian shape centered on the (100) plane. This diffraction affected behavior is evident in the profile of the Green function component $G_{11}(\mathbf{x},\omega)$ at 2 MHz as already shown in Fig. 5 of Sec. I.

To proceed further, we need to consider the individual Fourier components of the detected signals exemplified in Fig. 7. Figure 9 shows the typical Fourier spectra for the waveforms obtained at $x=0$ mm for the 15-, 25-, and 40-mm scan lines. A time window has been used which encloses only the SH mode FT signal that directly arrives from the source. It displays prominent peaks at approximately 1.9, 6.1, 8.1 MHz, which are somehow associated

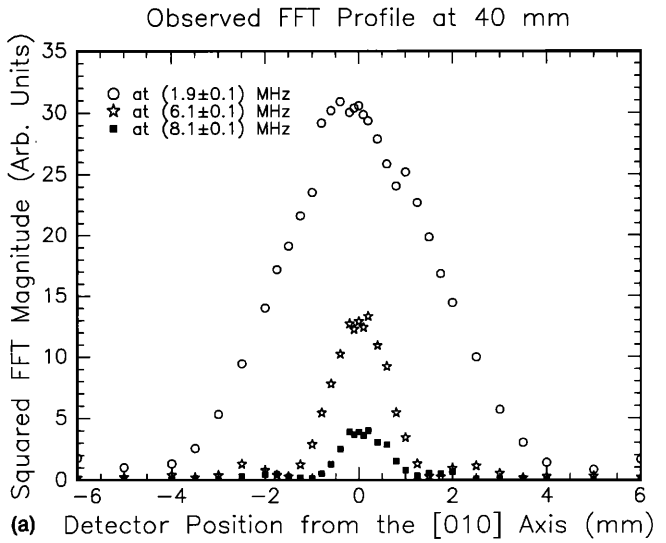

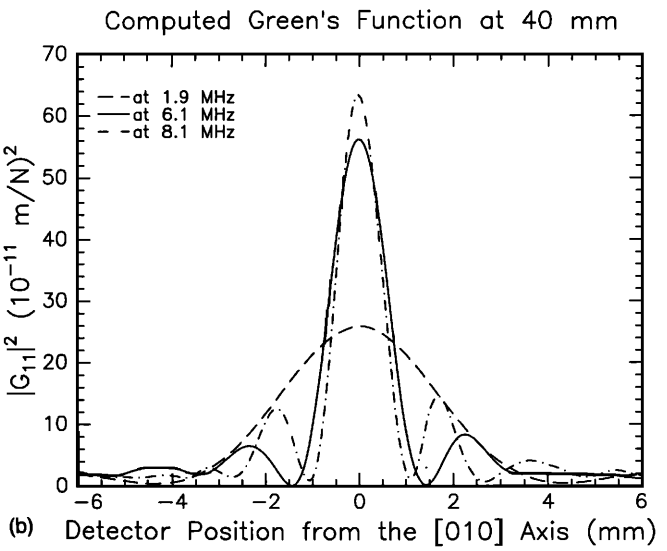

FIG. 10. Variation of the squared modulus of Fourier components at 1.9, 6.1, and 8.1 MHz with x on the scan line at 40 mm from epicenter: (a) observed and (b) computed.

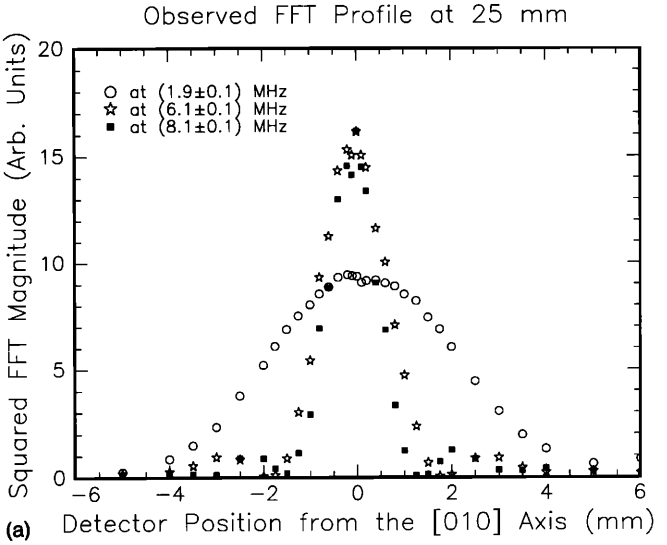

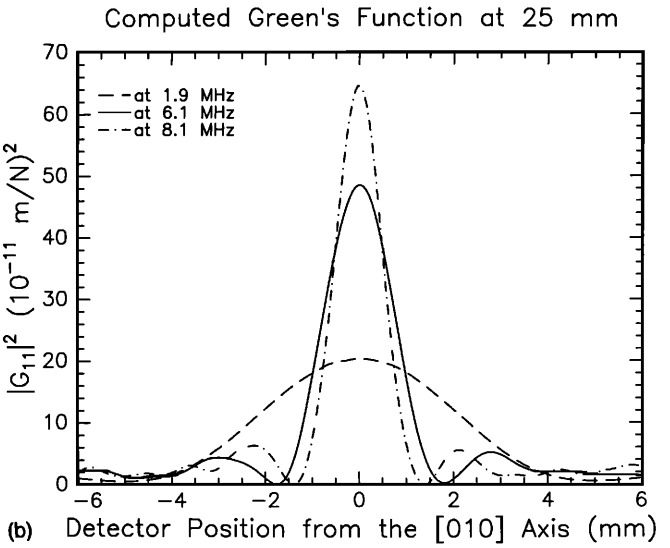

FIG. 11. Variation of the squared modulus of Fourier components at 1.9, 6.1, and 8.1 MHz with x on the scan line at 25 mm from epicenter: (a) observed and (b) computed.

with resonance of the transducers, a precise account of which is unnecessary for our purposes. The presence of the 6.1- and 8.1-MHz peaks in the figure may be due to the fact that the actual cutoff frequency of the amplifier used extends well above 10 MHz much higher than the −3-dB falloff frequecncy 2 MHz. The Fourier spectra of all the signals detected at various positions have been found to possess prominent peaks at almost the same frequencies as shown in Fig. 9, although they differ in magnitude. This is more or less consistent with Eq. (18), provided that $G_{11}(\mathbf{x},\omega)$ is a slowly varying function of ω in the ultrasonic frequency range at all the detector positions $\mathbf{x}$. The frequency spectrum of $G_{11}(\mathbf{x},\omega)$ at a particular position of $\mathbf{x}$ is entirely due to the impulse source acting at origin.

Figures 10–12 represent a detailed comparison between theory and experiment. Figure 10(a) shows the squared modulus of the 8.1-, 6.1-, and 1.9-MHz Fourier components of the observed waveforms as a function of x for a scan line at a 40-mm distance from the [001] axis. Each of these curves peaks at the center of the focusing ridge in the (100) plane, but they differ in width. The 8.1-MHz curve is the narrowest, having a half width of about 1 mm, a minimum at about 1.5 mm and then a small secondary peak at 2 mm. The 6.1-MHz curve shows very similar behavior except that the half-width is slightly broader and a small secondary peak appears at 2.5 mm. The 1.9-MHz curve is the broadest, with a half-width of about 3 mm. Only the relative variation of these intensities is significant and not their absolute magnitudes. Figure 10(b) shows the variation of $|G_{11}(\mathbf{x},\omega)|^2$, with x for the same three frequencies, with only the FT modes being included in the calculation. The calculated curves are in very good agreement with the Fourier components of measured waveforms with regard to the widths and positions of the various peaks and minima. This is also in accordance with the prediction of Eq. (18). Figure 11(a) and (b) shows similar data for a scan line at 25 mm from the [001] axis, and again there is good agreement between theory and

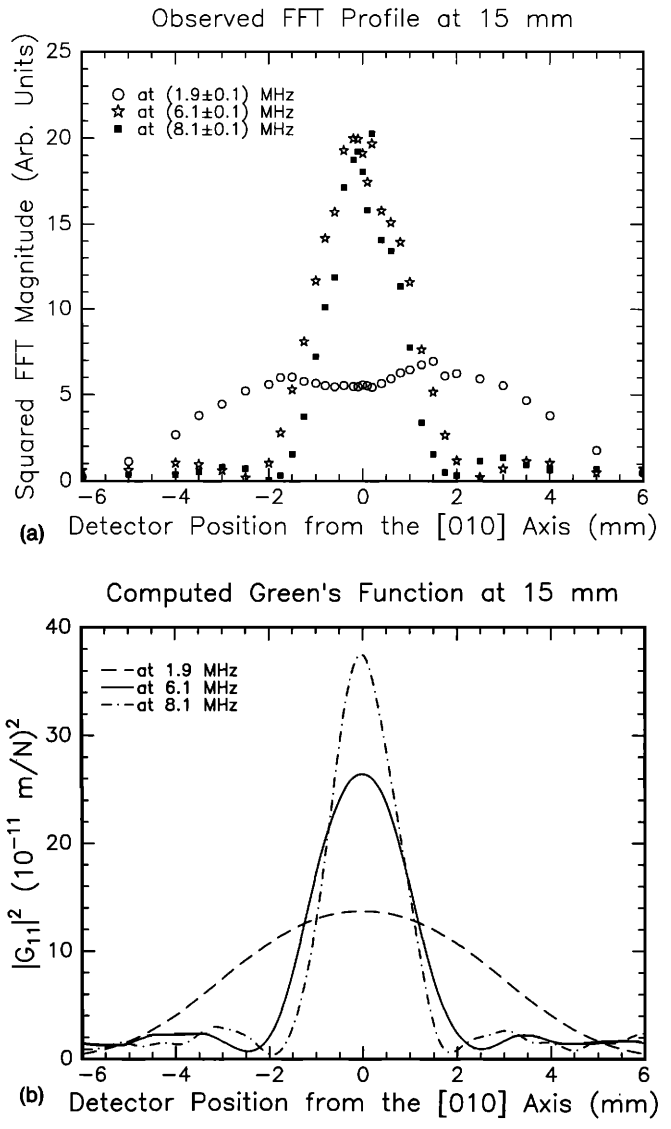

FIG. 12. Variation of the squared modulus of Fourier components at 1.9, 6.1, and 8.1 MHz with x on the scan line at 15 mm from epicenter: (a) observed and (b) computed.

experiment. Figure 12(a) and (b) shows corresponding data for a scan line at 15 mm from the [001] axis. In this case the 1.9-MHz curve displays a broad shallow depression near the center, which is well reproduced in the theory only when the ST modes are included in the calculation, as shown in Fig. 13. The reason for the necessity of doing this is, first, that near the [001] axis the FT and ST wave arrivals are very close to each other, and experimentally it is not possible to discriminate between them, and it is the combined signal that is Fourier transformed. Second, the reason the ST signal is there at all is because the 6-mm scan range extends far enough from the [010] axis that it is no longer only pure SH excitation that takes place. Furthermore, the ends of the scan line get well into the region of strong ST focusing.

IV. DISCUSSION

It is interesting to compare the FT mode focusing pattern of silicon with observations made on an elastically

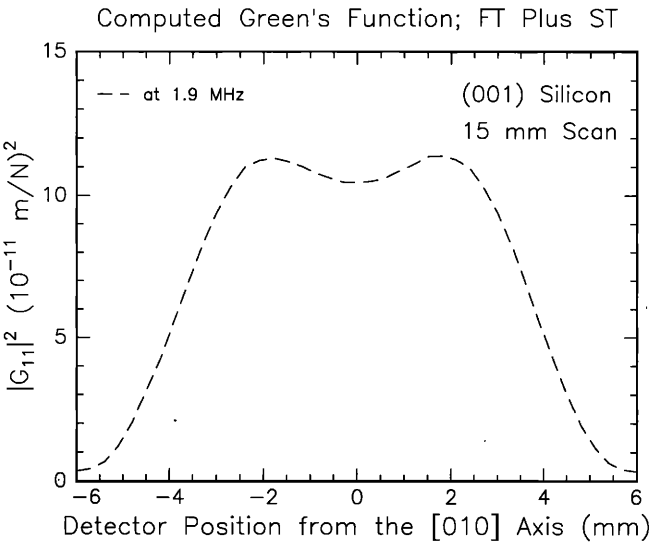

FIG. 13. Green's function at 1.9 MHz for the 15-mm scan line with both ST and FT modes included in the calculation.

isotropic sample in a similar experimental configuration. In an isotropic medium the longitudinal and transverse sheets of the slowness surface are both spherical in shape and the transverse sheet is doubly degenerate. There is no focusing in the sense discussed in this paper. The radiation pattern from a point source is not necessarily isotropic, however, but depends on the precise nature of the source, whether monopolar, dipolar, or combinational between these. The character of the source determines the relative amount of energy that is radiated into different wave normals for each branch. In the case of the degenerate transverse branches it is convenient to distinguish the modes as SH and sagittal in apportioning the energy.

We have performed an experiment with a 25.5-mm-thick isotropic glass plate using a shear source fixed both in position and in polarization on one side and a shear detector located at $\theta=45°$ on the other. We note here for clarity that the sagittal plane is defined by the normal to the glass plate and the source-to-detector direction. The source was polarized normal to the sagittal plane, while the detector polarization was rotated from $\varphi=-90°$ to $\varphi=90°$ with respect to this plane on the sample surface. Here, φ is an angle between the normal to the sagittal plane and the polarization of the detector. This is equivalent to scanning the detector in a semicircle of radius 25.5 mm centered at the epicenter, while the detector polarization is maintained tangential to this circle or normal to the sagittal plane. The measurements yield the SH radiation pattern for a fixed shear source. Figure 14 shows the observed angular dependence of the SH mode intensity normalized with respect to the intensity at $\varphi=0°$. The peak amplitude immediately after the arrival of the SH mode has been taken as a measure of intensity.

The distance from the source to the detector, which for all values of φ, is 36.06 mm, is far greater than a dominant wavelength 1.75 mm at 2 MHz, and corresponds to the far-field condition. In the far field of an isotropic medium, the theoretical intensity radiation pattern $I(\varphi)$ of SH

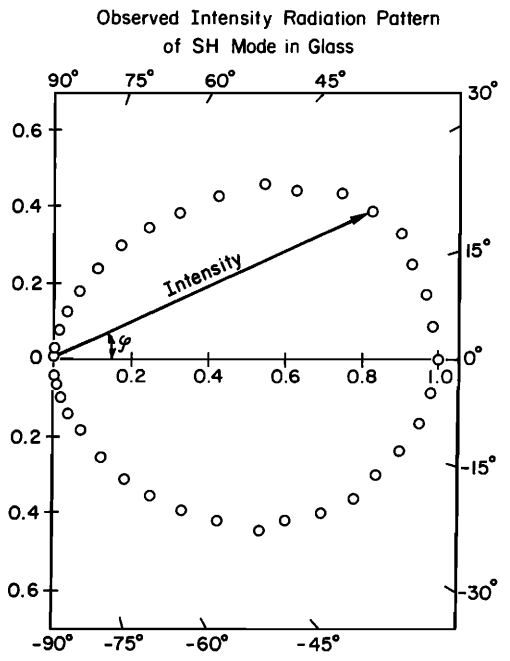

FIG. 14. A polar plot of the observed SH mode intensity radiation pattern in glass.

mode displacements polarized perpendicular to the sagittal plane is given by[26]

$$I(\varphi) \propto u_\varphi^2 \propto \frac{F^2(t)}{\mu^2 R^2} \cos^2 \varphi, \tag{19}$$

where μ is the shear modulus of an isotropic medium and R is the distance from the source to the detector. Equation (19) is independent of θ, as expected. For small values of φ there is only a very slight decrease in the intensity, quadratic in φ. This is due to source directivity, and signifies less energy being radiated into wave normals away from $\varphi=0°$. There is a similar source directivity to this for the FT modes in silicon near $\varphi=0°$, but it is masked by the very much more rapid variation of acoustic flux with φ due to focusing. At $\varphi=\pm 90°$ the SH intensity in glass approaches zero because of source directivity, and likewise the FT intensity in silicon also approaches zero at $\varphi=\pm 90°$ in spite of the intense focusing near this direction.

The SH mode described above is uncoupled from the quasilongitudinal (QL) and quasitransverse (QT) modes, both of which are, in general, sagittally polarized. The technique used in our experiment can be easily adapted to measure the group velocities of SH modes propagating in various directions in anisotropic media. Of particular interest are the SH modes propagating in the symmetry planes of media with orthorhombic or higher symmetry, as they are pure modes on these planes.[27] The SH mode arrival can be used for the determination of shear moduli of anisotropic media. Let us consider, for example, a broadband pulse of the pure SH mode polarized in the x_1 direction and propagating in the x_2x_3 symmetry plane at an angle θ to the x_3 axis of an orthorhombic medium. For this SH mode propagating at a group velocity V_g from a pointlike source to a pointlike detector, the following relation holds:

$$\frac{\sin^2\theta}{C_{66}} + \frac{\cos^2\theta}{C_{55}} = \frac{1}{\rho V_g^2}. \tag{20}$$

Using the similar relations for the x_1x_2- and x_1x_3 planes, all three shear moduli of the orthorhombic medium, C_{44}, C_{55}, and C_{66}, can be determined from the pure SH modes propagating in various directions in these symmetry planes. This provides a very convenient method of determining the shear moduli of anisotropic media, which may not be easily obtained either by using axisymmetric point sources or by other known conventional techniques. Using a pointlike source and pointlike detector, Kim *et al.* used Eq. (20) to determine the group velocity surface of the pure transverse mode and all five elastic constants of zinc.[30,31]

V. CONCLUSIONS

In conclusion, this paper demonstrates the strong focusing of FT ultrasonic waves in (001) oriented silicon, observed at room temperature with pointlike shear PZT transducers. We have shown that the anisotropic nature of the excitation, resulting from the [100] polarization of the transducers, breaks the fourfold symmetry in the focusing pattern of silicon, and strong focusing is confined to the vicinity of the (100) plane. Calculations of the elastodynamic Green's function of silicon account well for the spatial variation of the Fourier components of the observed signals at approximately 2, 6, and 8 MHz.

ACKNOWLEDGMENTS

The authors deeply appreciate the financial support received from the Physical Acoustics Division of the Office of Naval Research for this work.

[1] H. J. Maris, J. Acoust. Soc. Am. **50**, 812 (1971).
[2] G. A. Northrop and J. P. Wolfe, Phys. Rev. B **22**, 6196 (1980).
[3] H. J. Maris, in *Nonequilibrium Phonons in Nonmetallic Crystals*, edited by W. Eisenmenger and A. A. Kaplyanskii (North-Holland, Amsterdam, 1986), pp. 51–90.
[4] G. A. Northrop and J. P. Wolfe, in *Nonequilibriumm Phonon Dynamics*, edited by E. Bron (Plenum, New York, 1985), pp. 165–242.
[5] A. G. Every, "Thermal Phonon Imaging," in *Proceedings of the 29th Winter School in Theoretical Physics*, Poland, edited by T. Paszkiewicz and K. Rapcewicz (Plenum, New York, 1993) (in press).
[6] There is an exception to this. Through the phonon drag effect, it is possible to detect phonon momentum and observe "momentum focusing;" see C. Jasiukiewicz, D. Lehmann, and T. Paszkiewicz, Z. Phys. B **84**, 73 (1991); B **86**, 225 (1992).
[7] A. G. Every, W. Sachse, K. Y. Kim, and M. O. Thompson, Phys. Rev. Lett. **65**, 1446 (1990).
[8] A. G. Every and W. Sachse, Phys. Rev. B **44**, 6689 (1991).
[9] M. R. Hauser, R. L. Weaver, and J. P. Wolfe, Phys. Rev. Lett. **68**, 2604 (1992).
[10] R. L. Weaver, M. R. Hauser, and J. P. Wolfe, Z. Phys. B **90**, 27 (1993).
[11] J. Wesner, K. U. Wurz, K. Hillmann, and W. Grill, "Imaging of Coherent Phonons," in *7th International Conference on Phonon Scattering in Condensed Matter* VII, edited by M. Meissner and R. O. Pohl (Springer-Verlag, Berlin, 1993), p. 68.
[12] A. A. Kolomenskii and A. A. Maznev, JETP Lett. **53**, 423 (1991).
[13] K. Y. Kim and W. Sachse, in *IEEE 1992 Ultrasonics Symposium, Proceedings*, edited by B. R. McAvoy, sponsored by UFFC Soc., Vol. 2 (1992), pp. 1009–1013.

[14] K. Y. Kim, W. Sachse, and A. G. Every, Phys. Rev. Lett. **70**, 3443 (1993).
[15] V. T. Buchwald, Proc. R. Soc. Lond. Ser. A **253**, 563 (1959).
[16] G. F. D. Duff, Phil. Trans. Roy. Soc. **252**, 249 (1960).
[17] R. Burridge, Quart. J. Mech. Appl. Math., 41 (1967).
[18] N. Cameron and G. Eason, Quart. J. Mech. Appl. Math., 23 (1967).
[19] F. R. Yeatts, Phys. Rev. B **29**, 1674 (1984).
[20] A. Tverdokhlebov and J. Rose, J. Acoust. Soc. Am. **83**, 118 (1988).
[21] V. K. Tewary and C. M. Fortunko, J. Acoust. Soc. Am. **91**, 1888 (1992).
[22] R. G. Payton, *Elastic Wave Propagation in Transversely Isotropic Media* (Martinus Nijhoff, The Hague, 1983).
[23] M. G. Cottam and A. A. Maradudin, in *Surface Excitations*, edited by V. M. Agranovich and R. Loudin (Elsevier, Amsterdam, 1984).
[24] J. H. M. T. van der Hijden, *Propagation of Transient Elastic Waves in Stratified Anisotropic Media* (North-Holland, Amsterdam, 1987).
[25] A. G. Every, K. Y. Kim and W. Sachse, "Phonon Imaging at Ultrasonic Frequencies: The Dynamic Response of Anisotropic Solids," in *Proceedings of the 29th Winter School in Theoretical Physics*, Karpacz, Poland, edited by T. Paszkiewicz and K. Rapcewicz (Plenum, New York, 1993) (in press).
[26] K. Aki and P. G. Richards, *Quantitative Seismology* (Freeman, San Francisco, 1980), Vol. 1.
[27] M. J. P. Musgrave, *Crystal Acoustics* (Holden-Day, San Francisco, 1970).
[28] A. G. Every, Phys. Rev. B **22**, 1746 (1980).
[29] J. A. Shields and J. P. Wolfe, Z. Phys. B **75**, 11 (1989): J. A. Shields, J. P. Wolfe and S. Tamura, Z. Phys. B **76**, 295 (1989).
[30] K. Y. Kim and W. Sachse, J. Appl. Phys. **75**, 1435 (1994).
[31] K. Y. Kim and R. Sribar (to be published).